[Electronic Supplementary Information] Exploring Unconventional Ferromagnetism in Hole-doped LaCrAsO: Insights into Charge-Transfer and Magnetic Interactions

Zhao Liu[1, 2, *] and Nikhil V. Medhekar[1, 2, †]

[1] *Department of Materials Science and Engineering, Monash University, Victoria 3800, Australia*
[2] *ARC Centre of Excellent in Future Low-Energy Electronics Technologies, Monash University, Victoria 3800, Australia*

In this supplemental information, we provide more details of the calculations and results to support the main context. In Section A, we show SCAN + rVV10 describes LaCrAsO very well. In Section B, we explore the dopant-dopant interaction to illustrate that true $(La_{1-x}Sr_x)CrAsO$ alloy is preferred than phase separation. In Section C, the effect of hole doping on ε_{dp} is studied on the nonmagnetic phase. In Section D, the formation energy of FM SrCrAsO is discussed. In Section E, we exhaust possible exchange mechanisms and find that none of them play dominating roles in the itinerant FM at large x values. In Section F, the more advanced HSE06 functional is used to correct the half-metallic gap. In Section G, the self-doping phenomena is discussed. In Section H, we discuss how to calculate the magnetic phase transition temperature.

A. Performance of SCAN + rVV10 on LaCrAsO

As a parameter-free functional, SCAN can treat charge, spin and lattice degrees of freedom on equal footing and has shown great success in different types of bonding systems including cuprates [1, 2] which is the prototypical strongly correlated system. SCAN + rVV10 also shows good performance on LaCrAsO as discussed below.

The optimized lattice constant at C-type AFM phase is a = b = 4.049 Å, c = 9.003 Å, which is very close to the experimental X-ray diffraction value: a = b = 4.041 Å, c = 8.986 Å [3]. From the band structure displayed in Fig. S1(a), it is clear that LaCrAsO is metallic, in accordance with experiment [3]. To check the interlayer coupling, a 2×2×2 supercell is used. It is found that the G-type AFM has the lowest energy, in accordance with the experimental report [3]. It is noted that DFT + U method fails to capture G-type AFM as the ground state [3]. Park et al. [3] reported a local magnetic moment of 1.57 μ_B/Cr at room temperature. It is well known that thermal fluctuations make the local moments smaller than the saturated one. Since DFT calculations are based on zero temperature, it is reasonable that the calculated moments 3.23 μ_B/Cr is larger than 1.57 μ_B. Take LaMnAsO for example, it is reported that local moment of Mn^{2+} was observed to increase from 2.43 μ_B at 290 K to 3.34 μ_B at 2 K. Considering that Park et al. [3] didn't give the saturated magnetic moment of Cr^{2+}, here we turn to $Sr_2Cr_2AsO_3$ [4] and $Sr_2Cr_3As_2O_2$ [5] system for benchmark (both of which contains $[CrAs]^{1-}$ sublayer as in LaCrAsO). The saturated magnetic moment of Cr^{2+} is 2.68 and 3.37 μ_B, respectively. From these values, it is clear that: first of all, both the experiments and our calculations give magnetic moment smaller than the value expected from the high-spin configuration in the localized spin scheme (4 μ_B/Cr); secondly, the experimental data should be very close to 3 μ_B/Cr in LaCrAsO, which is not far from our calculation result.

To simulate the magnetic susceptibility curve, the exchange coupling strength (J) is needed. According to above analysis, it is reasonable to used effective $S = 3/2$ for energy mapping. Through energy mapping method,

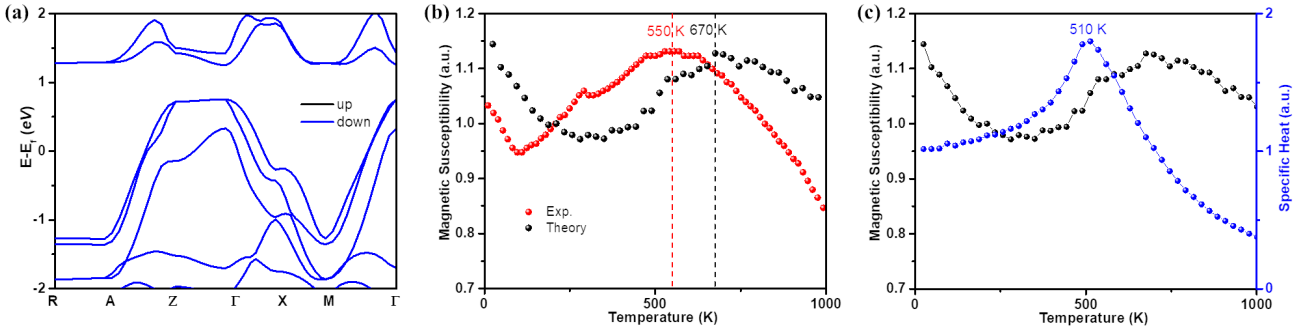

Figure S1: (a) Band structure of LaCrAsO in the C-type AFM phase. (b) Evolution of magnetic susceptibility with respect to temperature (black). Red: experimental data extracted from Park et al. [3]. (c) Theoretical simulation of magnetic susceptibility (black) and heat capacity (blue) with respect to temperature.

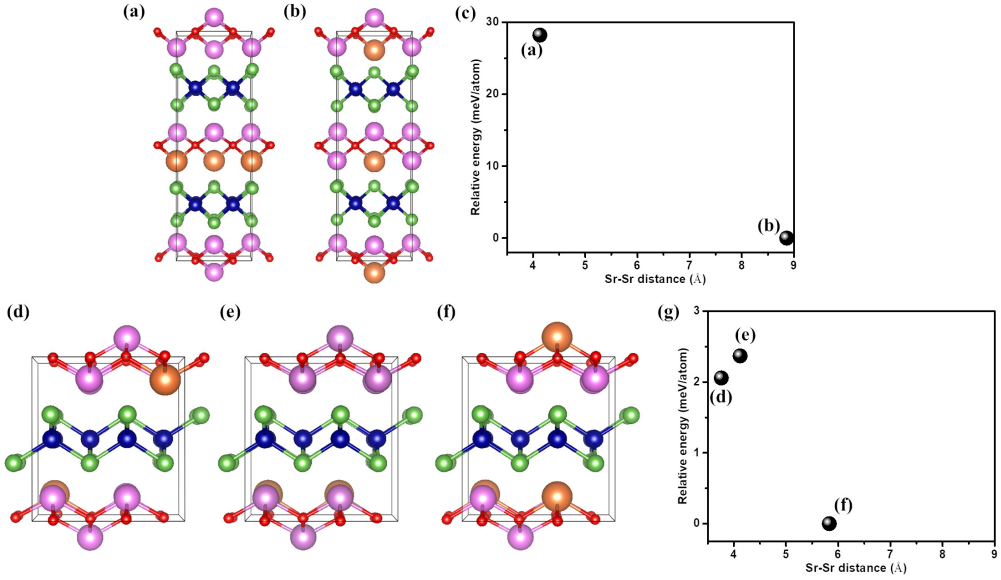

Figure S2: Dopant-dopant interactions in $(La_{0.75}Sr_{0.25})CrAsO$. (a, b) Two Sr atoms are in the same/different LaO sublayer in a $\sqrt{2}\times\sqrt{2}\times 2$ supercell. (c) Relative energy versus Sr-Sr distance for configuration (a) and (b). (d-f) Three inequivalent configurations for two Sr atoms in the same LaO sublayer in a $2\times 2\times 1$ supercell. (g) Relative energy versus Sr-Sr distance for configuration (d)-(f).

we calculated the nearest and next-nearest in-plane exchange coupling strengths to be J_1 = 19.27 meV, J_2 = -6.65 meV and the nearest out-of-plane exchange coupling strength to be $J_\perp$ = 0.12 meV. The positive $J_\perp$ confirm the antiferromagnetic coupling between adjacent CrAs sublayer along c direction. As $|J_2/J_1| < 0.5$, the system is frustration-free, in accordance with experiment [3]. After obtaining J_1 and J_2, we performed classical Monte Carlo (MC) simulations ($J_\perp$ is too small and hence ignored here). The result is shown in Fig. S1(b)-(c). In Fig. S1(b) we compare the magnetic susceptibility between experimental measurement and theoretical simulation. The broad maxima around 550 K in experimental data in Fig. S1(b) indicates 2D AFM nature in LaCrAsO [3], in accordance with our calculation result that $J_\perp \sim 0.1$ meV and hence, the validity of ignoring $J_\perp$ in MC simulation. The MC simulation gives a broad peak around 670 K, which is 120 K higher than the experimental reported 550 K. Despite this difference, the overall shape of theoretical magnetic susceptibility is in good accordance with the experimental one. Fig. S1(c) indicates that the Neel temperature (T_N) obtained by specific heat anomaly doesn't coincide with the peak given by magnetic susceptibility, confirming the assumption of Park et al. [3]. If we subtract a 120 K difference, the modified Neel temperature will be 390 K, which is in the region (300 K, 500 K) suggested by Park et al. [3].

In summary, SCAN + rVV10 show good performance in describing the lattice structure, electronic structure as well as the magnetic properties of LaCrAsO. Therefore, SCAN + rVV10 is used as the main functional in our manuscript.

B. Dopant-dopant interaction

Due to the facts that 1) the J_1/J_2 as well as the T_c keep increasing with x values growing; 2) the magnetic property at fully doping (x = 100%) is simulated in a unit cell, we can conclude that a large supercell than 2 × 2 × 1 won't affect the main physics here and the corresponding phase diagram should be similar to that of 2 × 2 × 1. Therefore, 2 × 2 × 1 supercell is large enough to explore the underlying mechanism.

To investigate whether the doped Sr atoms form a uniform solid solution or a separate phase, here we study the Sr-Sr interaction in the $x = 0.25$ system. Firstly, we use a $\sqrt{2}\times\sqrt{2}\times 2$ to see the interlayer interaction. In Fig. S2(a)-(b), two Sr atoms are placed in one and two LaO sublayers, where the optimized Sr-Sr distance is 4.13 and 8.86 Å, respectively. As shown in Fig. S2(c), the configuration shown in Fig. S2(a) has a much higher energy than the configuration in Fig. S2(b), indicating Sr atoms prefer to evenly distribute in LaO sublayers. This fact allows us to simulate $(La_{1-x}Sr_x)CrAsO$ in a supercell without repetition in the c direction. Secondly, we apply a $2\times 2\times 1$ supercell to investigate the intralayer interaction. The three inequivalent configurations are depicted in Fig. S2(d)-(f); note that Fig. S2(a) and Fig. S2(e) have same Sr-Sr distance. We have checked that all these three configurations have ferromagnetism as the ground state. Compared with interlayer interaction,

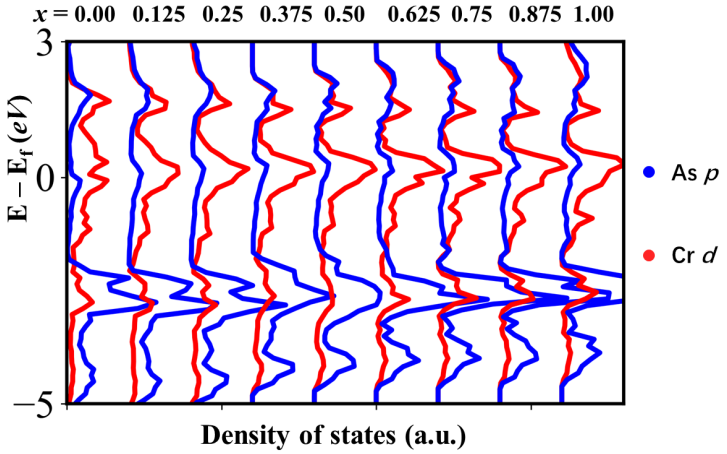

Figure S3: Element-resolved density of states for the nonmagnetic phase of $(La_{1-x}Sr_x)CrAsO$ at different x values.

Table I: Formation energy of $Sr_xCr_yAs_mO_n$ crystal

System	E_f (eV/atom)
2213	-3.03
2322	-1.66
2323	-1.94
1111	-1.42

the three different intralayer configurations have much smaller energy difference, the largest energy difference is only about 2.5 meV/atom (see Fig. S2(g)). As shown in Fig. S2(g), it is clear that Sr atoms also try to stay as far as possible from each other. In other words, Sr atoms also prefer to be evenly distributed in the intralayer direction. Furthermore, we have also checked that at $x = 0.75$, the two La atoms are also evenly distributed.

Combining both interlayer and interlayer dopant-dopant interaction, we draw the conclusion that the doped dopants will form a uniform $(La_{1-x}Sr_x)CrAsO$ alloy.

C. Effect of hole doping on ε_{dp}

Fig. S3 shows the partial density of states for Cr $3d$/As $4p$ orbitals for nonmagnetic phase at different x values. Compared with Cr $3d$ orbitals, As $4p$ orbitals undergo a blue shift to higher energy. In other words, the onsite energy difference between Cr $3d$ and As $4p$ ε_{dp} gradually decreases with increasing x.

D. Stability of $(La_{1-x}Sr_x)CrAsO$ alloys

Firstly we study the formation energy of FM SrCrAsO. For crystals $Sr_xCr_yAs_mO_n$, there are three experimentally synthesized systems: 2213 [4, 6], 2322 [5, 7], and 2323 [4], whose structures are displayed in Fig. S4. They all shared layer structure and there are $[CrAs]^{1-}$ sublayers in 2213 and 2322, which is the building block of 1111 studied in our work. Since SrCrAsO hasn't been synthesized, here the formation energies of 2213, 2322, 2323, and 1111 are calculated to see whether 1111 can be synthesized or not. Here the formation energy is defined as:

$$E_f = \frac{1}{x+y+m+n}[E(Sr_xCr_yAs_mO_n) - x\mu(Sr) - y\mu(Cr) - m(As) - \frac{n}{2}\mu(O_2)] \quad \text{(S1)}$$

where $E(Sr_xCr_yAs_mO_n)$ is the DFT energy of a magnetic supercell made of x Sr, y Cr, m As and n O atoms. $\mu(A)$ is the chemical potential of element A, here crystalline Sr, Cr and grey As, as well as triplet O_2 molecule are used to calculate the chemical potentials. E_f for different systems are listed in Tab. I. From Tab. I, it is clear that all these systems have negative formation energy; what is more, 1111 system has E_f close to that of 2322 system.

Secondly we check the dynamical and thermal stability of FM SrCrAsO. Fig. S4(d) shows the AIMD simulation at 300 K. From the fluctuation of temperature, 1000 fs is enough for a $4 \times 4 \times 2$ supercell to achieve thermal equilibrium. Without any structural breaking, the small energy fluctuations strongly suggest the thermal stability

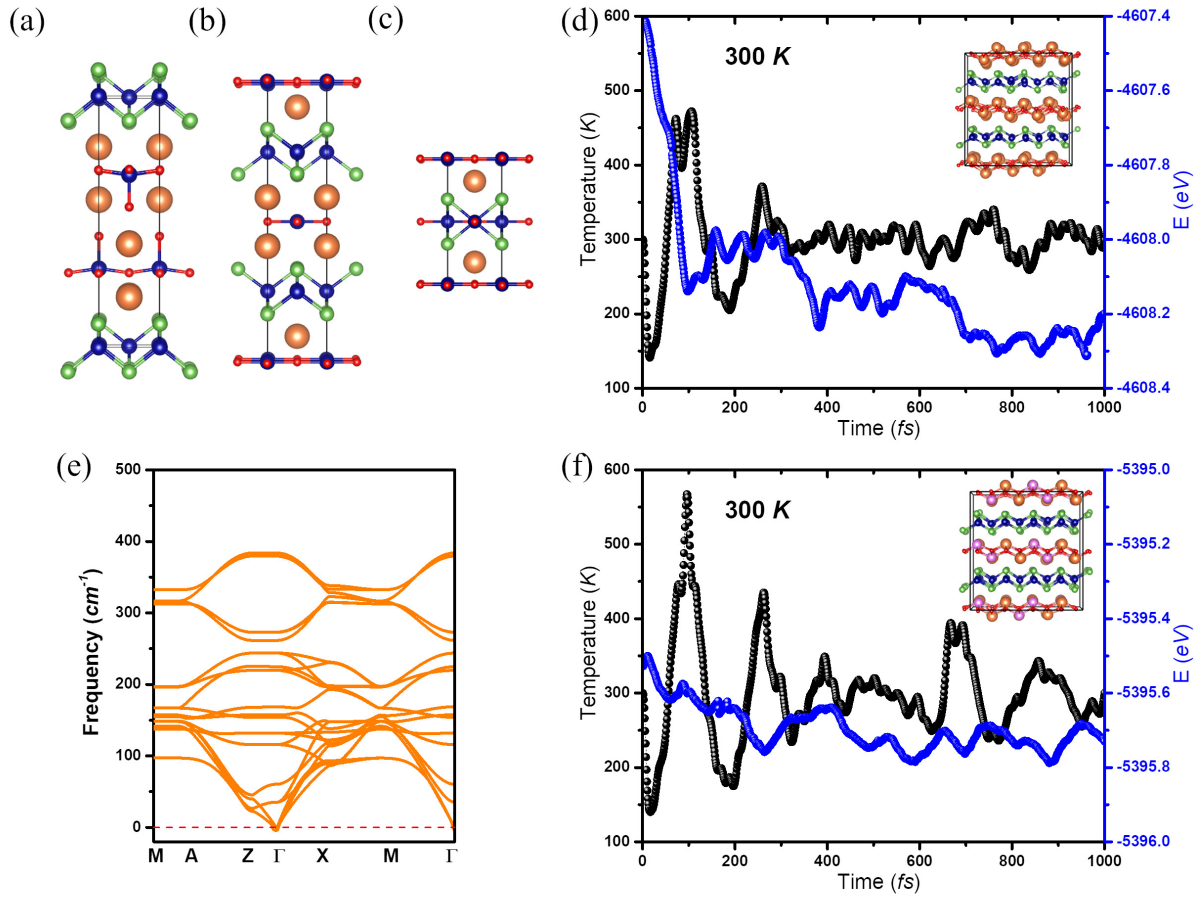

Figure S4: Perspective view of (a) 2213 (b) 2322 and (c) 2323. (d) AIMD simulation at 300 K for a $4 \times 4 \times 2$ supercell with SCAN functional at x = 1.00. Inset: perspective view of the last snapshot in the simulation. (e) Phonon spectrum of $(La_{0.5}Sr_{0.5})CrAsO$. (f) AIMD simulation at 300 K for a $2 \times 2 \times 2$ supercell with SCAN functional at x = 0.50. Inset: perspective view of the last snapshot in the simulation.

of SrCrAsO. Combined with the phonon spectrum in Fig. 2(c) in the main context, it is strongly indicated that SrCrAsO can exist as a 3D crystal. The dynamical and thermal stability of $(La_{1-x}Sr_x)CrAsO$ alloys are also checked by taking $x = 0.50$ as an example. Fig. S4(e) shows the phonon spectrum and Fig. S4(f) displays the AIMD simulation at 300 K. Just like SrCrAsO, no imaginary modes present in Fig. S4(e) and no structural reconstruction is observed in Fig. S4(f) with small energy fluctuations.

Combining all above results, $(La_{1-x}Sr_x)CrAsO$ alloys should be experimentally accessible.

E. Exclusion of common exchange mechanisms for the itinerant FM at large x values

In this section, we compare the intralayer exchange mechanism around $x = 1.00$ with existing ones, including superexchange, double exchange, extended superexchange, multi-intermediate double exchange, Stoner ferromagnetism and Ruderman-Kittle-Kasuya-Yosida (RKKY) mechanism.

E-I. Superexchange mechanism

The superexchange interaction can be reasonably estimated by a simple Cr-As-Cr model as shown in Fig. S5(a): there are two Cr atoms at sites i and j and one As atom at site k linking these two Cr atoms. The super-exchange coupling J_{ij} is the product of two processes: (1) a hopping process between d orbitals at site i and p orbitals at site k (see Fig. S5(b)); (2) an direct exchange process between p orbitals at site k and d orbitals

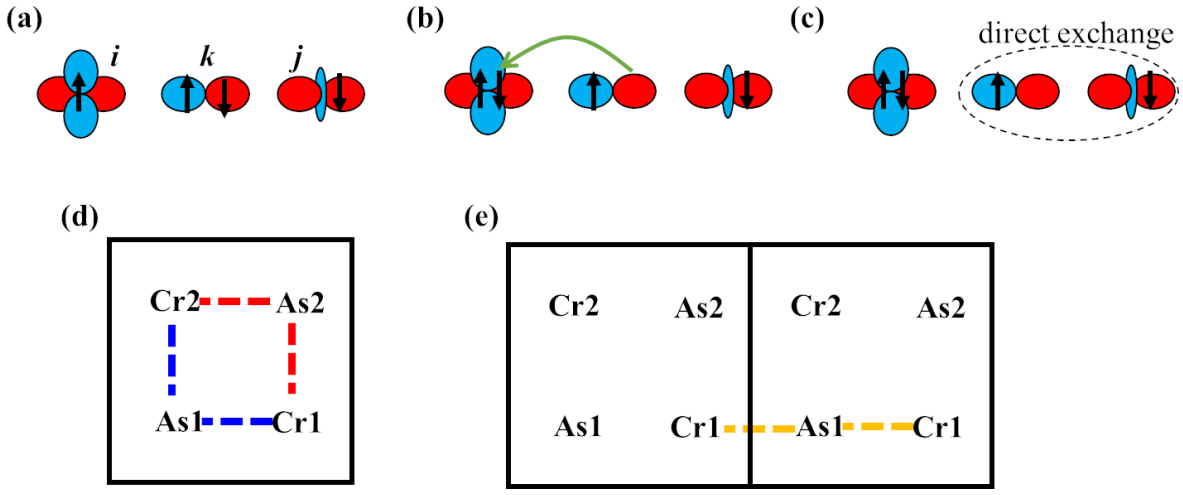

Figure S5: (a) Schematic of the superexchange interaction by a $d-p-d$ model. (b) The electronic configuration after an electron hopping from site k to site i (green arrow). (c) The direct exchange coupling between site k and site j is marked by the dashed circle. (d) For J_1 in CrAs sublayer, there are two paths connecting Cr1 and Cr2 as labelled by the blue and red dashed lines. (e) For J_2 in CrAs sublayer, there is only one path connecting Cr1 and equivalent Cr1 as labelled by the yellow dashed lines.

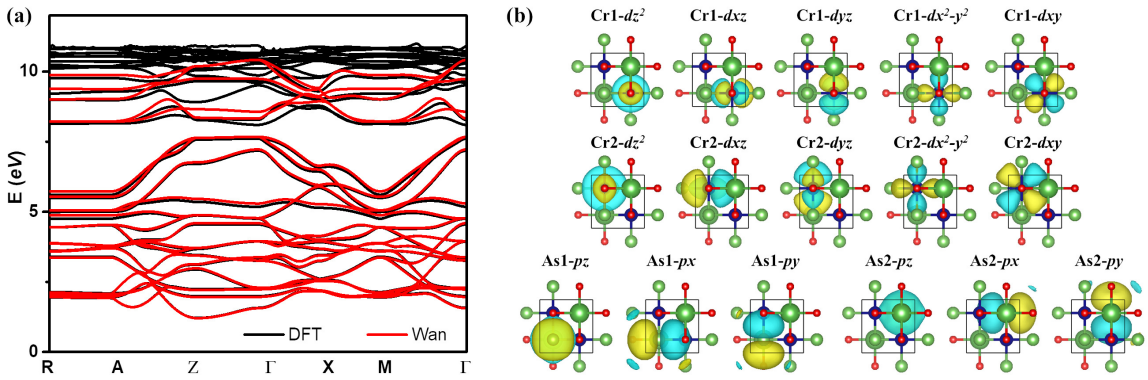

Figure S6: (a) DFT calculated (black) and Wannier fitted (red) band structures of LaCrAsO in the C-type AFM phase. (b) The representative maximally localized Wannier functions of the CrAs sublayer (O is also used in the downfolding, but the corresponding orbitals are not shown here). The isovalue of the isosurface is $\pm$ 1.00 Å$^{-3/2}$.

at site j (see Fig. S5(c)). These two processes give the following formula on J_{ij} [8, 9]:

$$J_{ij} = (\frac{1}{E^2_{i,\uparrow\downarrow}} - \frac{1}{E^2_{i,\uparrow\uparrow}}) \sum_k \sum_{p,d} \frac{2t^2_{id,kp} t^2_{kp,jd}}{|\varepsilon_{k,p} - \varepsilon_{j,d}|} \tag{S2}$$

where $E_{i,\uparrow\downarrow}, E_{i,\uparrow\uparrow}$ are energies of two d electrons at site i with anti-parallel and parallel spins; $t_{id,kp}$ ($t_{kp,jd}$) is the hopping strength between d orbital at site i and p orbital at site k (p orbital at site k and d orbital at site j); $\varepsilon_{k,p}$ ($\varepsilon_{j,d}$) is the onsite energy of p orbital at site k (d orbital at site j). It is noted that the summation over k in Eq. S2 means that all possible As atoms connecting two nearest Cr atoms should be considered, specifically, there are two As atoms for J_1 and one As atoms for J_2 (see Fig. S5(d)-(e)). Here we only interested in the ratio $|J_2/J_1|$, therefore we take $\frac{1}{E^2_{i,\uparrow\downarrow}} - \frac{1}{E^2_{i,\uparrow\uparrow}}$ as a pending parameter.

We first focus on LaCrAsO, whose AFM is believed to be the result of superexhchange mechansim. To see this point, Wannier downfolding is performed on the C-type AFM (here we focus on intralayer exchange coupling, so C-type AFM is applied instead of G-type). Shown in Fig. S6 there is a good match between DFT and Wannier fitted bands—what is more, the obtained Wannier orbitals well resemble the corresponding localized atomic orbitals.

The single-particle parameters including $t_{id,kp}$, $t_{kp,jd}$, $\varepsilon_{k,p}$ and $\varepsilon_{j,d}$ can be obtained from the above downfolding

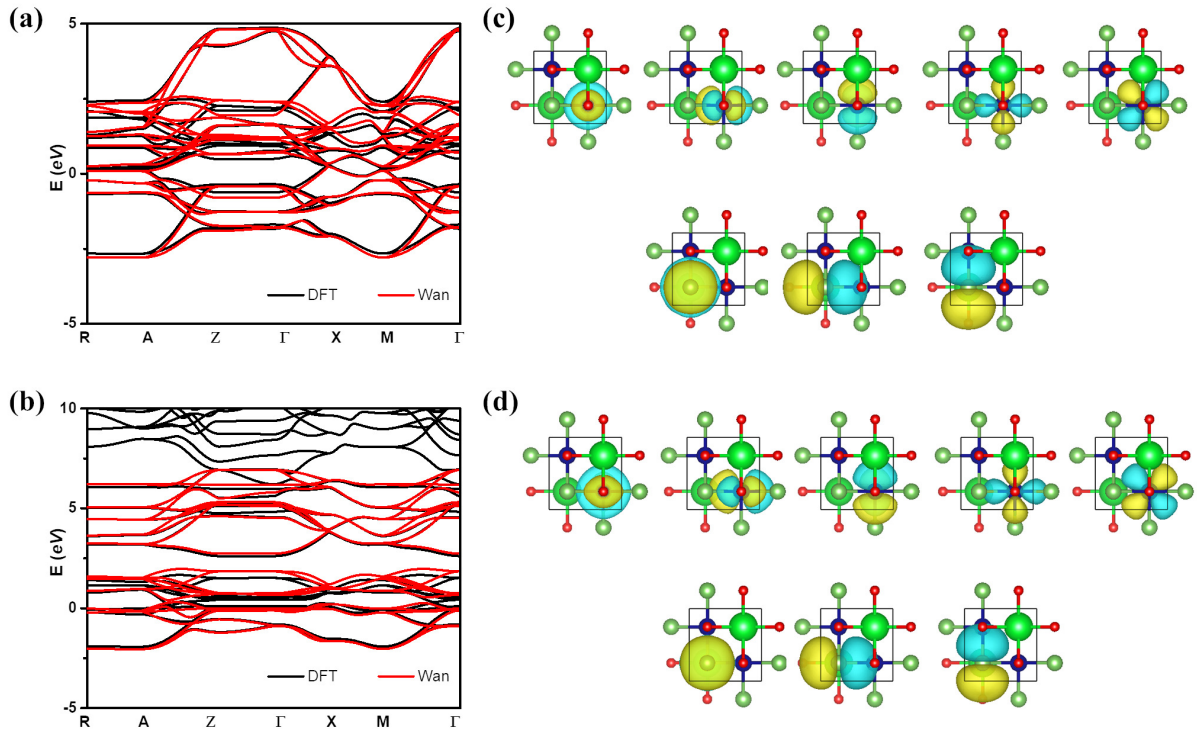

Figure S7: (a)-(b) DFT calculated (black) and Wannier fitted (red) band structures of SrCrAsO at the FM phase for spin up and down channel. (c)-(d) The representative maximally localized Wannier functions of the CrAs sublayer for spin up and down channel (O is also used in the downfolding, but the corresponding orbitals are not shown here). Because of symmetry, only half of the Cr $3d$/As $4p$-like MLWFs are shown here. The isovalue is ± 1.00 Å$^{-3/2}$.

process. By plugging these parameters into Eq. S2, we have $|J_2/J_1| = 0.33$. According to DFT calculations, we find that $|J_2/J_1| = 0.34$. These two values are very close to each other, confirming the dominant role of superexchange mechanism in LaCrAsO.

Then we turn to SrCrAsO and perform downfolding procedure on the FM phase. Shown in Fig. S7 there are a good match between DFT and Wannier fitted bands in both spin channels, and the obtained Wannier orbitals resemble the corresponding localized atomic orbitals very well. By plugging the fitted parameters into Eq. S2, we have $|J_2/J_1| = 0.50$. According to DFT calculations, we find that $|J_2/J_1| = 1.11$. Therefore, superexchange mechanism can't be the prevailing origin of FM in SrCrAsO.

To gain more information about the sign of $|J_2/J_1|$ in superexchange mechanism, here we also study a similar system: LaMnAsO. LaMnAsO has the same crystal structure as LaCrAsO and the ground state is also C-type AFM (see Fig. S8(a)), as a result of superexchange mechanism. The lattice constants calculated by SCAN + rVV10 are a = b = 4.086 Å, c = 8.983 Å, which is very close to the experimental value: a = b = 4.124 Å, c = 9.030 Å [10]. The calculated band gap of C-type AFM phase is 0.85 eV (see Fig. S8(b)), not far from the experimental one ($\sim$ 1.4 eV) [11]. Now we consider the fully hole-doped case (SrMnAsO), the ground state is still C-type AFM as shown in Fig. S8(a). The reentrant AFM at $x = 1.00$ resembles the situation in $LaMnO_3$, indicating that superexchange mechanism dominates near both $n = 0.00$ and 1.00. Considering the similarity between LaCrAsO and LaMnAsO, we can conclude that if superexchange mechanism dominates in SrCrAsO, J_2/J_1 should be -0.50, which is far away from the DFT calculated $J_2/J_1 = 1.11$. Therefore, superexchange mechanism can't explain the FM exchange interactions in SrCrAsO.

E-II. Canonical double exchange mechanism

Here we argue that the FM at around $x = 1.00$ can't be explained by the CDE mechanism. The main reason is, according to CDE mechanism, T_c peaks at an optimal doping concentration x_c and after x_c the CDE becomes weaker and weaker and finally superexchange mechanism dominates again. However, this is not what we observed for $x > 0.20$ where the FM becomes stronger.

Despite this, there is a related mechanism called "self-doped double exchange", proposed by Korotin et al. [12]

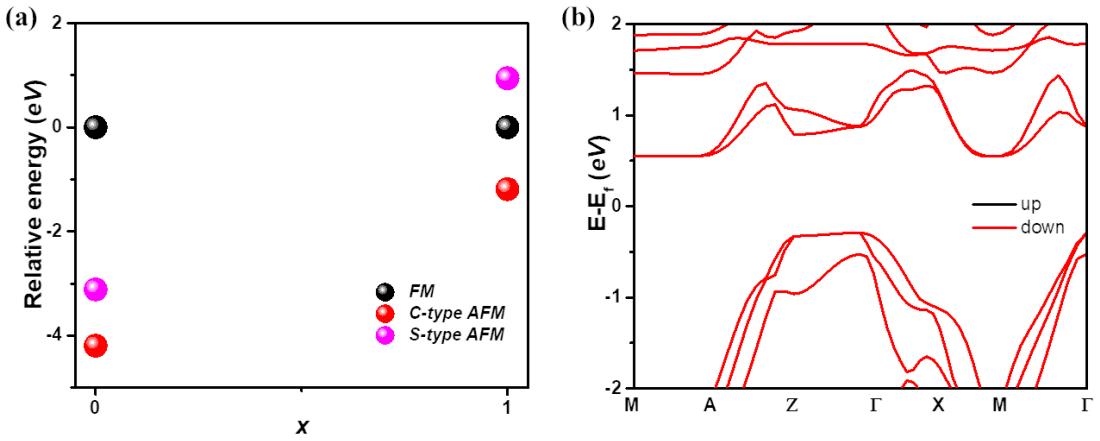

Figure S8: (a) Phase diagram for hole doped LaMnAsO. (b) Band structure of LaMnAsO at C-type AFM phase.

in the study of itinerant ferromagnet CrO_2. But we find such a name is misleading because it implies that such a mechanism can only work in itinerant FM. According to our analysis, it is highly possible that the phases $x = 1.00$ is a ferromagnetic negative charge-transfer energy insulator and we can still observe the unsaturated T_c until $x = 1.00$. In this sense the requirement of itinerancy is not a prerequisite for the strong FM.

Combing these above two arguments, we believe that the CDE mechanism is not the main reason for the strong FM in SrCrAsO.

E-III. Extended superexchange mechanism

To explain the high T_c in 2D ferromagnetic insulator CrOCl [13], an extended superexchange mechanism was proposed by Zhang et al. [14]. In this theory, polyvalent anions (like O^{2-} and Cl^{1-} in CrOCl) are very important to break Goodenough-Kanamori-Anderson semiempirical rules [15–18]. Since there is only one type of anions in CrAs sublayer, such a mechanism doesn't play a role here.

E-IV. Multi-intermediate double exchange interaction

In 2020, Wang et al. [19] reported a novel multi-intermediate double exchange interaction in bilayer ferromagnets. The Bethe-Slater-curve-like behavior offers a distance-dependent interlayer AFM to FM transition. Because there is no bilayer structure in SrCrAsO, we don't expect such a mechanism to work here.

E-V. Stoner ferromagnetism

Stoner mechanism describes the competition between electron exchange and kinetic energy in an itinerant system. If the former dominates, the system is FM, otherwise PM is favored. Such a mechanism is featured by the following characteristics: (1) the magnetic moment is not localized, but delocalized; (2) the band structures for the spin up and down channels are quite similar, only differed by a rigid band shift; (3) AFM order is hard to converge in such kind of systems. Although SrCrAsO is metallic, it shows none of the above features, and consequently, Stoner ferromagnetism plays minor roles.

E-VI. RKKY mechanism

RKKY is a peculiar form of exchange interaction that occurs in metals with localized magnetic moments [20–22]. In this picture, a localized magnetic moments polarize surrounding conduction electrons, and such polarization in turn couples to another neighboring localized magnetic moments. The coupling strength takes the form of distance-dependent exchange interaction, which can be either FM or AFM. In SrCrAsO here, we note that RKKY can't be dominating due to the following two reasons: (1) with $x > 0.20$, the density of carriers

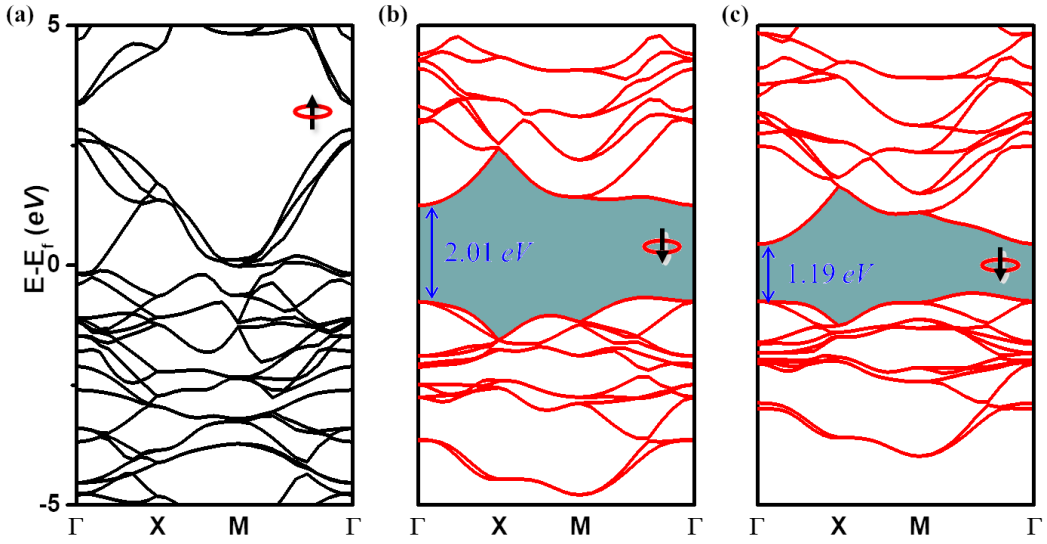

Figure S9: (a, b) Magnetic band structure of SrCrAsO in the spin up/down channel at the HSE06 functional level. (c) Magnetic band structure of SrCrAsO in the spin down channel at the SCAN functional level.

varies and both AFM and FM J should be observed, but only FM J is observed; (2) In RKKY picture, J not only fluctuates but also decays, if both J_1 and J_2 are FM, then J_2 should be much smaller than J_1. However, for $x > 0.20$, J_2 is much larger than J_1.

E-VII. Flat-band and partially flat-band ferromagnetism

Recall that Stoner criterion U$\rho_F > 1$ (ρ_F is the density of state at Fermi level), there are two ways to realize such a criterion. The first one is setting U $\to \infty$, which just gives the Nagaokaâs theorem. Since U $\to \infty$ can never be realized in real materials, such a theorem doesnât work here. The second one is setting $\rho_F \to \infty$, which can be realized in materials with flat-band or partial flat-band structures. Since there are no flat bands at Fermi level for all doping concentrations shown in Fig. S3, such a mechanism wonât be the dominating one.

F. HSE06 band structure of SrCrAsO

In our previous work [23], we mentioned that HSE06 functional is a good choice for the study of ferromagnetic negative charge-transfer energy insulator. Nevertheless, $(La_{1-x}Sr_x)CrAsO$ at different x values are all metallic. Under such circumstances, hybrid functional is not a good choice, but can be applied to correct the half-metallic gap.

Fig. S9(a)-(b) shows the spin up/down band structure of SrCrAsO on the HSE06 functional level. It is clear that spin up is gapless while spin down has a large gap, confirming the half-metallic nature. Fig. S9(c) displays the spin down band structure of SrCrAsO on the SCAN functional level. Comparing Fig. S9(b) and Fig. S9(c), we know HSE06 functional gives $\sim +0.80$ eV correction to the half-metallic gap.

G. Self-doping phenomena in SrCrAsO

Fig. S10(a)-(b) display the orbital resolved band structure of FM SrCrAsO in the spin up and down channel, both by setting the hopping terms between Cr d and As + O p orbitals to zero. It is clear that spin up and spin down channel share different features. In the spin down channel, As + O p orbitals are fully occupied while Cr d orbitals are empty, which satisfy the condition for positive charge-transfer energy. As for the spin up channel, As + O p overlap with Cr d orbitals. The fact that almost pure p states extend to the Fermi level is quite important. This means that these states can be used as electron or hole reservoirs, leading to "self-doping" phenomena [12].

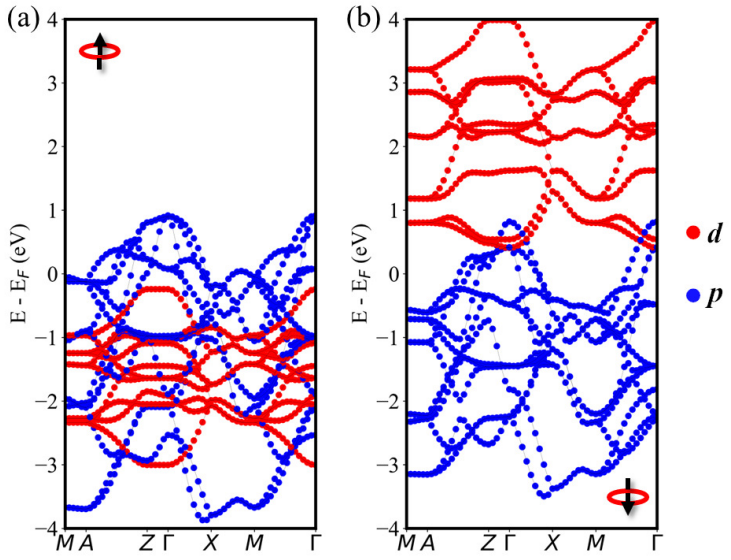

Figure S10: (a, b) Orbital resolved band structure of FM SrCrAsO without hopping terms between Cr d and As + O p orbitals in the spin up and down channel. The red/blue dot represents Cr d/As + O p orbitals respectively.

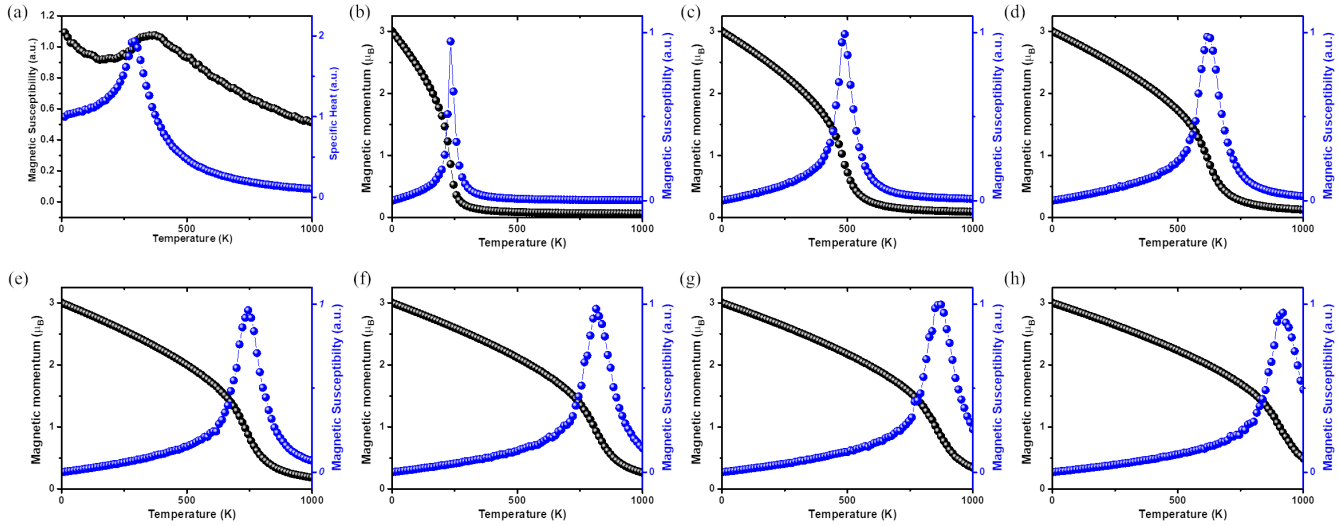

Figure S11: (a) At $x = 0.125$, the evolution of magnetic susceptibility (black) and heat capacity (blue) with respect to temperature. (b)-(h) At $x = 0.25$, 0.375, 0.50, 0.625, 0.75, 0.825, and 1.00, the evolution of magnetic moment (black) and magnetic susceptibility (blue) with respect to temperature.

H. Determination of phase transition temperature

The determination of phase transition temperature is a two-step process. Firstly, energy mapping method was applied to calculate J. Secondly, classical Monte Carlo simulations were performed based on spin model.

The spin model used here is the Heisenberg model:

$$H = \sum_{i,j} J_{ij} \vec{S}_i \cdot \vec{S}_j \tag{S3}$$

where summation is over nearest neighbor (J_1) and next-nearest neighbor (J_2) exchange coupling constant. And the energy for the three magnetic orders in the main context are calculated as:

$$\begin{aligned} E_{\mathrm{FM}} &= E_0 + 16J_1S^2 + 16J_2S^2 \\ E_{\mathrm{C-type\ AFM}} &= E_0 - 16J_1S^2 + 16J_2S^2 \\ E_{\mathrm{S-type\ AFM}} &= E_0 - 16J_2S^2 \end{aligned} \tag{S4}$$

where E_0 is a reference energy. By taking E_{FM}, $E_{\mathrm{C-type\,AFM}}$ and $E_{\mathrm{S-type\,AFM}}$ into above equations, J_1 and J_2 can be obtained for $S = 3/2$. Here we need to stress that S at different x values are all close to 3/2 although the formal oxidation state of Cr in LaCrAsO/SrCrAsO is 2+/3+, respectively. At $x = 0.00$, although high-spin configuration in the localized spin scheme gives 4 μ_B/Cr for Cr^{2+}, both experimental results and our calculations gives $S = 3/2$. At $x = 1.00$, formally we have Cr^{3+} which again leads to $S = 3/2$. We can perform energy mapping for all x values and the obtained J_1 and J_2 are shown in Fig. 3(a) in the main context.

With J_1 and J_2 obtained, classical Monte Carlo simulations are performed. During FM-PM phase transition ($x = 0.25$, 0.375, 0.50, 0.625, 0.75, 0.825, and 1.00), magnetic susceptibility is calculated after the systems reach equilibrium at a given temperature, then T_c corresponds to the positions of peak in magnetic susceptibility plot as shown in Fig. S11(b)-(h). For AFM-PM phase transition ($x = 0.125$), the phase transition temperatures determined by the magnetic susceptibility and specific heat still have disparity, just like the case in LaCrAsO. Here we choose T_N to be the peak position of specific heat curve in in Fig. S11(a).

* Electronic address: Zhao.Liu@monash.edu
† Electronic address: Nikhil.Medhekar@monash.edu

[1] C. Lane, J. W. Furness, I. G. Buda, Y. Zhang, R. S. Markiewicz, B. Barbiellini, J. Sun, and A. Bansil, *Phys. Rev. B* **98**, 125140 (2018).
[2] Y. Zhang, C. Lane, J. W. Furness, B. Barbiellini, J. P. Perdew, R. S. Markiewicz, A. Bansil, and J. Sun, *Proc. Natl. Acad. Sci. U.S.A.* **117**, 68-72 (2020).
[3] S.-W. Park, H. Mizoguchi, K. Kodama, S.-i. Shamoto, T. Otomo, S. Matsuishi, T. Kamiya, and H. Hosono, *Inorg. Chem.* **52**, 13363 (2013).
[4] B. C. Sheath, X. Xu, P. Manuel, J. Hadermann, M. Batuk, J. O'Sullivan, R. S. Bonilla, and S. J. Clarke *Inorg. Chem.* **61**, 13363 (2022).
[5] X. Xu, M. A. Jones, S. J. Cassidy, P. Manuel, F. Orlandi, M. Batuk, J. Hadermann, and S. J. Clarke *Inorg. Chem.* **59**, 15898 (2020).
[6] Y.-Q. Lin, H. Jiang, H.-X. Li, S.-H. Song, S.-Q. Wu, Z. Ren, and G.-H. Cao *Materials* **15**, 802 (2022).
[7] J. Liu, J. Wang, J. Sheng, F. Ye, K. M. Taddei, J. A. Fernandez-Baca, W. Luo, G.-A. Sun, Z.-G. Wang, H. Jiang, G.-H. Cao, and W. Bao *Phys. Rev. B* **98**, 134416 (2018).
[8] D. S. Dai, and K. M. Qian, Ferromagnetism, Vol. 1. *(Science Press, Beijing, 2017).*
[9] J.-W. Li, Z. Zhang, J.-Y. You, B. Gu, and G. Su, *Phys. Rev. B* **107**, 224411 (2023).
[10] A. T. Nientiedt, W. Jeitschko, P. G. Pollmeier, and M. Brylak, *Z. Naturforsch B* **52**, 560-564 (1997).
[11] K. Kayanuma, H. Hiramatsu, T. Kamiya, M. Hirano, and H. Hosono, *J. Appl. Phys.* **105**, 079303 (2009).
[12] M. A. Korotin, V. I. Anisimov, D. I. Khomskii and G. A. Sawatzky, *Phys. Rev. Lett.* **80**, 4305 (1998).
[13] N. Miao, B. Xu, L. Zhu, J. Zhou, and Z. Sun, *J. Am. Chem. Soc.* **140**, 2417-2420 (2018).
[14] F. Zhang, Y.-C. Kong, R. Pang, L. Hu, P.-L. Gong, X.-Q. Shi, and Z.-L. Tang, *New J. Phys.* **21**, 053033 (2019).
[15] J. B. Goodenough, *Phys. Rev.* **100**, 564 (1955).
[16] J. B. Goodenough, *J. Phys. Chem. Solids* **6**, 287 (1958).
[17] J. Kanamori, *J. Phys. Chem. Solids* **10**, 87-89 (1959).
[18] P. W. Anderson, *Phys. Rev.* **115**, 2 (1959).
[19] C. Wang, X. Zhou, L. Zhou, Y. Pan, Z.-Y. Lu, X. Wan, X. Wang, and W. Ji, *Phys. Rev. B* **102**, 020402(R) (2020).
[20] M. A. Ruderman, and C. Kittel, *Phys. Rev.* **96**, 99 (1954).
[21] T. Kasuya, *Prog. Theor. Phys.* **16**, 45 (1956).
[22] K. Yoshida, *Phys. Rev.* **106**, 893 (1957).
[23] Z. Liu, X. Li, W. Zhu, Z. F. Wang, and J. Yang, *Phys. Rev. B* **107**, 014413 (2023).